ADVANCED MATERIALS
www.advmat.de

Transforming Weakness into Strength: Photothermal-Therapy-Induced Inflammation Enhanced Cytopharmaceutical Chemotherapy as a Combination Anticancer Treatment

Lei Zhang, Ying Zhang, Yanan Xue, Yue Wu, Qianqian Wang, Lingjing Xue, Zhigui Su, and Can Zhang**

A new synergistic treatment that combines photothermal therapy (PTT) and inflammation-mediated active targeting (IMAT) chemotherapy based on cyto-pharmaceuticals is developed. During PTT, the photothermal tumor ablation is accompanied by an inflammatory effect and upregulation of inflammatory factors at the tumor site, which may accelerate tumor regeneration. Moreover, PTT-induced inflammation can also recruit neutrophils (NEs) to the tumor site. To convert the disadvantages of PTT-induced inflammation into strengths, NEs are investigated as cytopharmaceuticals for IMAT chemotherapy to further inhibit the tumor recurrence after PTT due to the chemotaxis of NEs to the inflammatory sites. In this study, PEGylated gold nanorods (PEG-GNRs) are explored as the photothermal agent and paclitaxel-loaded cytopharmaceuticals of NEs as the IMAT chemotherapeutic agent. PTT is conducted at 72 h postinjection of PEG-GNRs, followed by cytopharmaceuticals for IMAT chemotherapy. It is demonstrated that the cytopharmaceuticals effectively accumulate in the tumor sites after PTT, which leads to a significant enhancement of antitumor efficacy and a reduction in systemic toxicity. These studies suggest that PTT-induced inflammation further enhances the chemotherapy of cytopharmaceuticals, and the combination of PTT and IMAT chemotherapy may be a promising synergistic strategy for targeted cancer therapy.

Recent evidence has emerged suggesting that the combination of different treatments for anticancer therapy displayed favorable prospects compared to the individual therapeutic model.[1] These combination strategies could improve the overall efficacy, particularly in elevating the survival rate, restraining cancer recurrence and metastasis, reducing drug side effects, and overcoming drug resistance, in cancer patients. Photothermal therapy (PTT) in combination with chemotherapy has attracted substantial attention as an effective approach for cancer treatment.[2] During PTT, the energy of near-infrared (NIR) light was converted to heat by photothermal agents after irradiation at target sites, which could provide a spatiotemporally thermal effect to ablate the cancer tissues within the light-irradiated region, resulting in specific therapeutic effects with no damage to normal tissues.[2c,3] However, the use of PTT alone is virtually impossible to eliminate cancer cells due to the heterogeneous distribution of heat within the cancer tissue.[4] The surviving cancer cells from PTT will further lead to cancer relapse and metastasis.[5] Moreover, it has been shown that the cancer ablation process of PTT could lead to serious cell necrosis and produce an inflammatory response,[2c,5a,6] followed by the release of inflammatory factors, such as TNF-α, IL-1β, IL-6, IL-8, and IL-10,[7] which can prime neutrophils (NEs) to migrate to the inflamed tumor area.[8] In addition, another case reported that PTT-induced inflammation might accelerate tumor regeneration.[9] Given that both primary and metastatic cancer cells could be suppressed by chemotherapy, the combination of PTT and chemotherapy may be a superior strategy for cancer treatment.

Recently, our group demonstrated that cytopharmaceuticals based on NEs loaded with nanomedicine for chemotherapy could be recruited into the brain after cancer resection through inflammation-mediated active targeting (IMAT) and significantly suppressed the recurrence of glioma in mice.[10] IMAT chemotherapy based on cyto-pharmaceuticals loaded with nanomedicine was attributed to the gradient of chemoattractants between the injection site and the inflammatory tumor site, which was completely different from the conventional cancer-active delivery nanomedicine based on the recognition and binding of the targeting moieties to cell-surface markers.[10,11] In addition, the interactions between cytopharmaceuticals and inflammatory factors would be effective and specific as a result of their intact biological activities. Furthermore, the interactions between targeting moieties and cell-surface markers would be

L. Zhang, Y. Zhang, Y. N. Xue, Y. Wu, Q. Q. Wang, Dr. L. J. Xue, Dr. Z. G. Su, Prof. C. Zhang
State Key Laboratory of Natural Medicines
Jiangsu Key Laboratory of Drug Discovery for Metabolic Diseases
Center of Advanced Pharmaceuticals and Biomaterials
China Pharmaceutical University
No. 24 Tongjiaxiang, Nanjing 210009, China
E-mail: zhiguisu707@cpu.edu.cn; zhangcan@cpu.edu.cn

The ORCID identification number(s) for the author(s) of this article can be found under https://doi.org/10.1002/adma.201805936.

DOI: 10.1002/adma.201805936

hindered by the distribution, density, or spatial conformation of targeting moieties on the surface of nanomedicine because the cell-surface markers were dynamic rather than static.[12] Therefore, IMAT chemotherapy based on cytopharmaceuticals could overcome the limitations of conventional cancer-active delivery nanomedicine.

Inflammation plays an essential role in IMAT chemotherapy. To turn the weakness of PTT-induced inflammation into advantages, we sought to explore PTT-induced inflammation for the recruitment of cytopharmaceuticals based on NEs into tumor sites to inhibit tumor reoccurrence after PPT. Moreover, the upregulation of TNF-α in tumor sites after PTT could stimulate NEs to form neutrophil extracellular traps (NETs),[13] leading to the release of cargo from NEs. With the active recruitment and stimulated drug release of PTT-induced inflammation, combining PTT and cytopharmaceuticals based on NEs would provide an advantageous, synergistic cancer therapy with minimal systemic side effects. To this end, we herein report a new synergetic anticancer system that combined PTT and IMAT chemotherapy utilizing PEGylated gold nanorods (PEG-GNRs) as photothermal agents[14] and paclitaxel (PTX)-loaded cytopharmaceuticals (PTX-CL/NEs) as the IMAT chemotherapeutic agent. The PTT was conducted with laser irradiation after the accumulation of PEG-GNRs in cancer for cancer ablation accompanied by proinflammatory responses.[15] PTX-CL/NEs were subsequently administered by intravenous injection and actively recruited to cancer sites by the chemotactic effect of PTT-induced inflammation. The highly activated PTX-CL/NEs in cancer sites were expected to release intact PTX-CL along with NET formation. The cationic charges of PTX-CL enhanced the uptake by residual cancer cells for a further boosted cancer expunge (**Figure 1**).

The PEG-GNRs were prepared as synthesized gold nanorods with methoxy-PEG-thiol (MW 5 kDa), which has a unitary morphology with an aspect ratio of 4/1 and a UV absorbance at ≈808 nm (Figure S1A,B, Supporting Information). PEG-GNRs were highly stable in vitro within 72 h when incubated in H_2O, phosphate buffered saline (PBS), or 50% serum (Figure S2, Supporting Information), and there were no plasmon resonance peak shifts in the UV–vis absorption spectrum of the PEG-GNRs before incubation (0 h) and after incubation (72 h) with different media (Figure S3, Supporting Information). Furthermore, PEG-GNRs exhibited distinct photothermal effects after laser irradiation compared with saline; stronger photothermal effects occurred using 2 W cm^{-2} as the hyperthermic condition compared to 1 W cm^{-2} (Figure S4, Supporting Information). These results indicated that PEG-GNRs used for PTT could have satisfactory stability and photothermal effects in vitro, which would be beneficial to its biological performance in vivo. The pharmacokinetic profile and biodistribution of PEG-GNRs in mice were also investigated. Due mainly to the PEG coating, PEG-GNRs presented a satisfactory plasma stability with a plasma half-life of ≈17 h (Table S1, Supporting Information). 72 h postinjection, ≈95% of the PEG-GNRs were eliminated from the blood, and most of the PEG-GNRs distributed into tissues. This long circulation property also ensured the efficient accumulation of PEG-GNRs in cancer at 72 h postinjection through an enhanced permeability and retention (EPR) effect, and ≈7%ID of PEG-GNRs could be found in cancer tissues as determined by inductively coupled plasma–mass spectrometry (ICP-MS) (Figure S1C,D, Supporting Information).[16]

To evaluate the PTT of PEG-GNRs in vivo, HepS tumor-bearing mice were intravenously injected with PEG-GNRs (10 mg kg^{-1} calculated by Au), and the tumor region was exposed to 1 or 2 W cm^{-2} laser irradiation for different time periods after 72 h postinjection and monitored with an infrared thermal camera. As shown in **Figure 2**A, the PEG-GNRs group showed a more significant increase in temperature than the saline group under the same conditions. The temperature increase at the tumor sites of the PEG-GNRs group was also more conspicuous compared to the saline group (Figure 2B,C). The plateau temperature in the PEG-GNRs group was ≈42 and 46 °C after exposure to 1 or 2 W cm^{-2} laser irradiation, respectively, for 5 min. In addition, the photothermal ablation of PEG-GNRs was visualized by 2,3,5-triphenyltetrazolium chloride (TTC) staining.[17] A more serious necrosis was observed after exposure to 2 W cm^{-2} laser irradiation for 5 min (Figure 2D), which confirmed the PTT efficacy of PEG-GNRs.

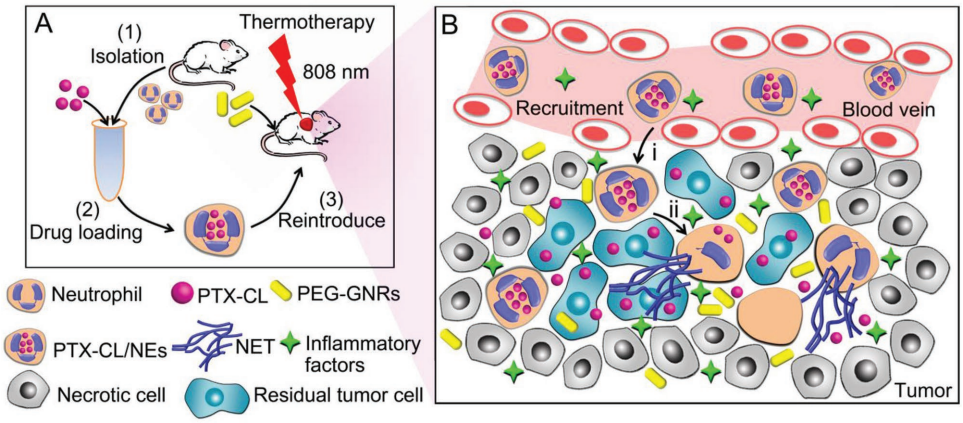

Figure 1. Schematic illustration of synergetic anticancer system combining PTT and inflammation-mediated active targeting chemotherapy. A) Schematic illustration of PTX-CL/NE preparation and the procedure of administration, including intravenous injection of PEG-GNRs, conduction of PTT, and reintroduction of PTX-CL/NEs. B) Schematic illustration of the chemotactic effect of PTT-induced inflammation to recruit PTX-CL/NEs to tumor sites (i) and stimulated drug release of PTX-CL from PTX-CL/NEs along with NET formation (ii).

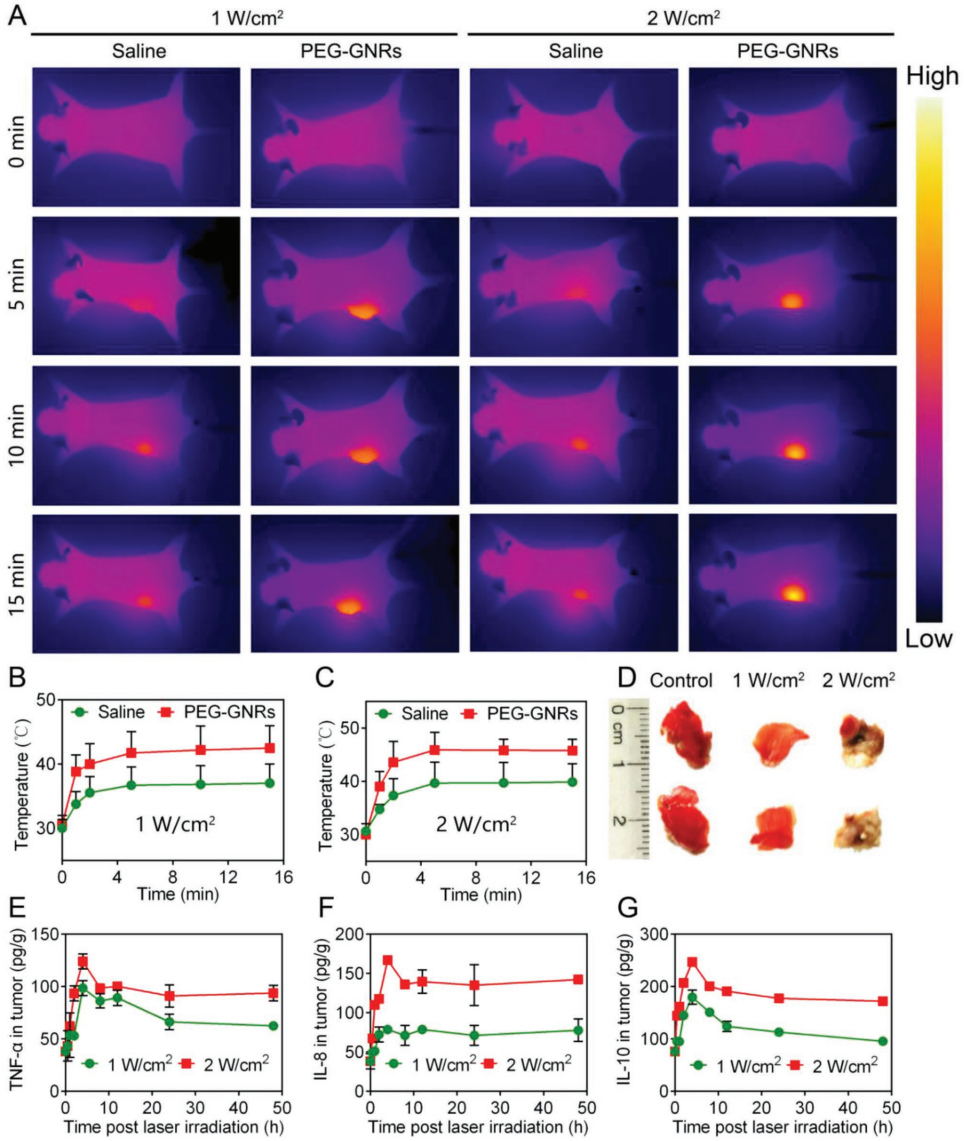

Figure 2. The PTT and inflammation stimulation of PEG-GNRs. A) Infrared thermal images of HepS-tumor-bearing mice at 1 or 2 W cm^{-2} for different times. B,C) The change of temperature at the tumor site under 1 or 2 W cm^{-2} irradiation monitored with an infrared thermal camera. The data are shown as the mean ± s.d. ($n = 3$). D) The photothermal effect induced tumor cell necrosis after 5 min irradiation, visualized by TTC staining. PEG-GNRs injected tumor-bearing mice without irradiation were dedicated as the control. E–G) The ELISA analysis of inflammatory factor (TNF-α, IL-8, and IL-10) expression in tumor tissues ($n = 2$ independent experiments).

The expression levels of inflammatory factors (TNF-α, IL-8, and IL-10) associated with the chemotactic migration of NEs after PTT at various time points were evaluated using enzyme-linked immunosorbent assay (ELISA). As shown in Figure 2E–G, the inflammatory factors in the tumor tissues significantly increased after PTT compared to without laser irradiation. The upregulation of inflammatory factors was attributed to the PEG-GNRs-mediated hyperthermic ablation, which caused necrosis of tumor cells and the release of necrotic debris, ultimately leading to the proinflammatory response.[2c] Taken together, these results illustrated that the tumor cells were expunged through PTT after PEG-GNRs accumulation at tumor sites and upregulated inflammatory factors, which could induce the chemotactic migration of drug-loaded NEs toward the residual cancer cells. To obtain the maximal thermotherapeutic effects, the hyperthermic condition in this study was fixed at 2 W cm^{-2} for 5 min post 72 h administration of PEG-GNRs. Furthermore, the PTT-induced inflammation in this hyperthermic condition could be exploited to recruit NEs to tumor sites.

For IMAT chemotherapy, the cytopharmaceuticals based on NEs were prepared and confirmed as previously reported by our group.[10] Briefly, the PTX-loaded cationic liposome (PTX-CL) was prepared by a standard thin film/extrusion method and then incubated with freshly harvested NEs to obtain PTX-CL/NEs. As shown in Figure S5 (Supporting Information), compared to Taxol (commercial PTX formulation) that exhibited a greater cytotoxicity at a high concentration of PTX, PTX-CL had no

cytotoxicity toward NEs at all assessed concentrations within 8 h incubation, which could facilitate NEs to load with PTX-CL. The intact physiological functions of NEs after loading with PTX-CL were evaluated, including the specific protein expression, chemotaxis, and superoxide-generating ability. Both of them were similar to the blank NEs. Moreover, the PTX-CL/NEs showed satisfactory stability in a normal physiological environment and the chemotactic process while displaying a burst release under inflammatory simulation.[10] To investigate whether PTX-CL loading would affect the in vivo behaviors of NEs, NEs, or PTX-CL/NEs were labeled with the fluorescence dye of DiR to prepare DiR-NEs and PTX-CL/DiR-NEs. After intravenous injection in BALB/C mice, the fluorescence intensity of DiR in the blood was determined. Both the in vivo fluorescence images and the overtime curve of the mean fluorescence intensity (MFI) indicated that DiR-NEs and PTX-CL/DiR-NEs exhibited similar pharmacokinetic behaviors within 48 h (Figures S6 and S7, Supporting Information). The half-life of the DiR-NEs and

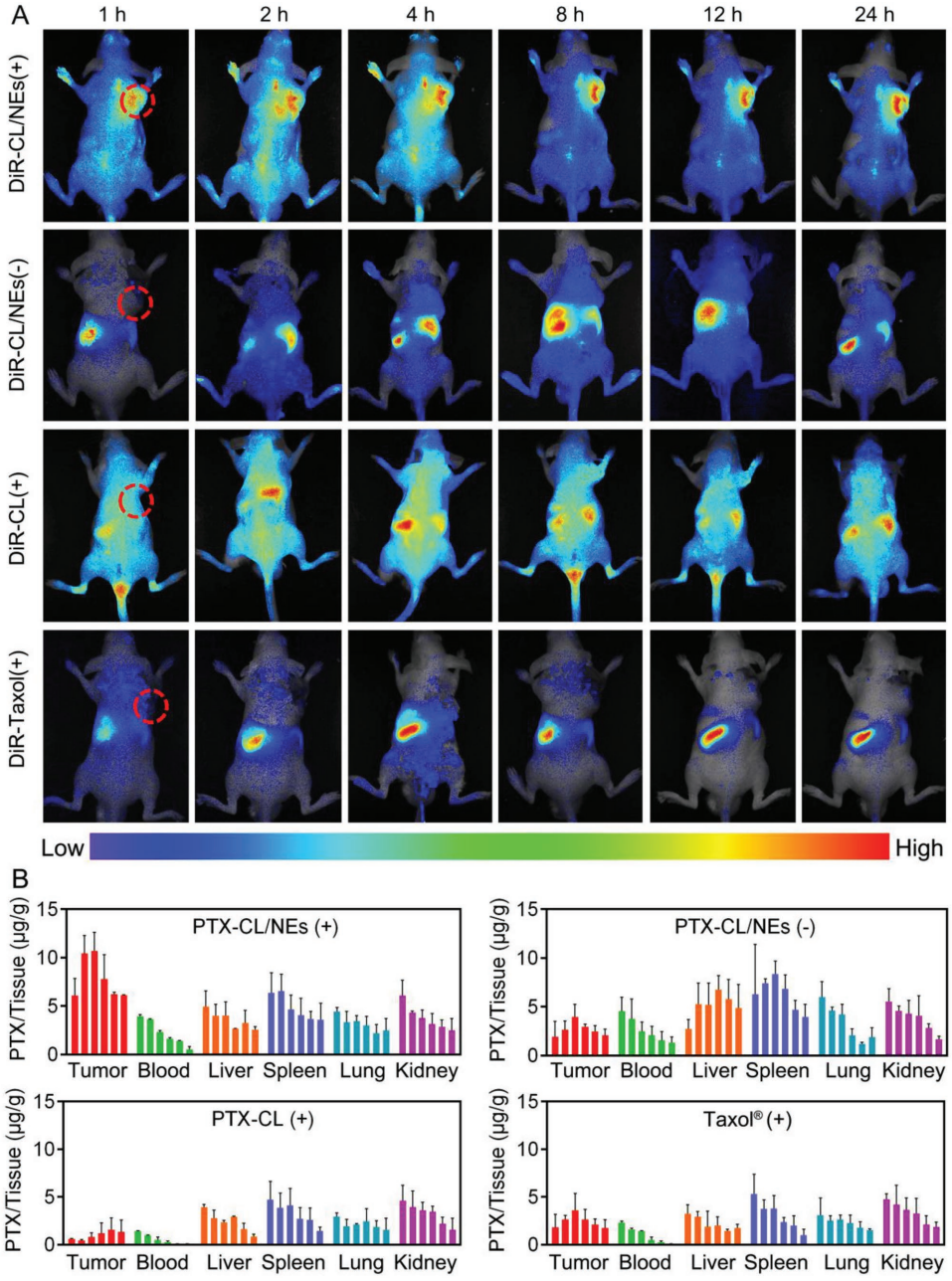

Figure 3. Inflammation-mediated active targeting of PTX-CL/NEs. A) Fluorescence image of HepS-tumor-bearing mice. DiR-CL, cationic liposome loaded with DiR (1,1′-dioctadecyl-3,3,3′,3′-tetramethylindotricarbocyanine iodide); DiR-CL/NEs, NEs loaded with DiR-CL; DiR-Taxol, DiR-labeled Taxol. B) Biodistribution profiles of PTX-CL/NEs, PTX-CL, and Taxol in HepS-tumor-bearing mice. All mice were administered PEG-GNRs and treated with (+) or without (–) 808 nm laser irradiation at 72 h postinjection of PEG-GNRs. Tissue samples were harvested at 1, 2, 4, 8, 12, and 24 h after intravenous injection. PTX/tissue was the ratio of the amount of PTX in the tissue (μg) to the weight of the tissue (g). The data are shown as the mean ± s.d. ($n = 3$).

PTX-CL/DiR-NEs was ≈20.37 ± 0.5 and 20.06 ± 0.23 h, respectively, which indicates that PTX-CL loading would not affect the physiological functions of NEs in vivo. To investigate the IMAT of drug-loaded NEs, the fluorescence dye of DiR was loaded into the cationic liposomes (DiR-CL) for constructing DiR-CL/NEs. PEG-GNRs were first intravenously injected into HepS-tumor-bearing mice, and the tumor lesion was exposed to 2 W cm^{-2} 808 nm laser irradiation for 5 min at 72 h postinjection. DiR-CL/NEs were then intravenously injected, and in vivo fluorescence imaging was applied to trace the chemotactic migration of DiR-CL/NEs. As shown in **Figure 3**A, after 1 h postinjection, a strong fluorescence signal of DiR-CL/NEs was observed at the tumor site and could remain for 24 h. In contrast, a negligible fluorescence signal was detected at the tumor sites of the mice after intravenous injection of DiR-CL/NEs without laser irradiation (Figure 3A, second row). In addition, the mice treated with DiR-CL or DiR-Taxol after photothermal therapy (Figure 3A, third and fourth rows) did not show a tumor targeting capability. These findings suggested that NEs have the advantage of carrying cargoes toward the inflammatory tumor site induced by PTT. Moreover, the biodistribution of PTX-CL/NEs at different time points after intravenous injection was also detected (Figure 3B). Similar results were obtained as the in vivo fluorescence imaging, and PTX-CL/NEs exhibited a maximum accumulation of PTX at cancer tissues after PTT, which further confirmed the IMAT of PTX-CL/NEs in vivo.

To investigate the duration of IMAT for drug-loaded NEs after one-time PTT, HepS-tumor-bearing mice received DiR-CL/NEs at different time points and were monitored by in vivo fluorescence images. The results confirmed that the accumulation of DiR-CL/NEs in the tumor sites was time-dependent (**Figure 4**). Both the in vivo fluorescence image and the analysis of the MFI within the tumor sites indicated that the highest fluorescence signal occurred on the 2nd d and became weak as time prolonged to the 8th d; after the 10th d post-PTT, the fluorescence signal of the DiR-CL/NEs in the tumor was too weak to detect (Figure 4A,B). The hold duration suggested that the chemotactic effect of one-time PTT could sustain for ≈8 d for recruiting DiR-CL/NEs toward tumor sites. IL-8 was considered to be the primary chemokine for NE chemotaxis.[18] The duration of IL-8 expression after one-time PTT in the tumor, liver, and spleen was determined by ELISA assay (Figure 4C). A higher level of IL-8 was found at the tumor tissues than in the liver or spleen at all time points, which would enhance the recruitment of DiR-CL/NEs to the tumor and efficiently avoid the nonspecific distribution of DiR-CL/NEs in the liver or spleen. The highest level of IL-8 in the tumor occurred from day 2 to day 3 post PTT, and the amount of IL-8 then gradually decreased. The tendency of the IL-8 expression in the tumor sites was similar to the in vivo fluorescence imaging of the duration of IMAT for DiR-CL/NEs after PTT. Taken together, these data illustrated that the hold IMAT of drug-loaded NEs should be within the 8th d post one-time PTT, and the maximal IMAT of drug-loaded NEs would occur at ≈2 d post one-time PTT.

Given that drug-loaded NEs could accumulate in cancer sites by IMAT, the cargoes transferred from drug-loaded NEs to cancer

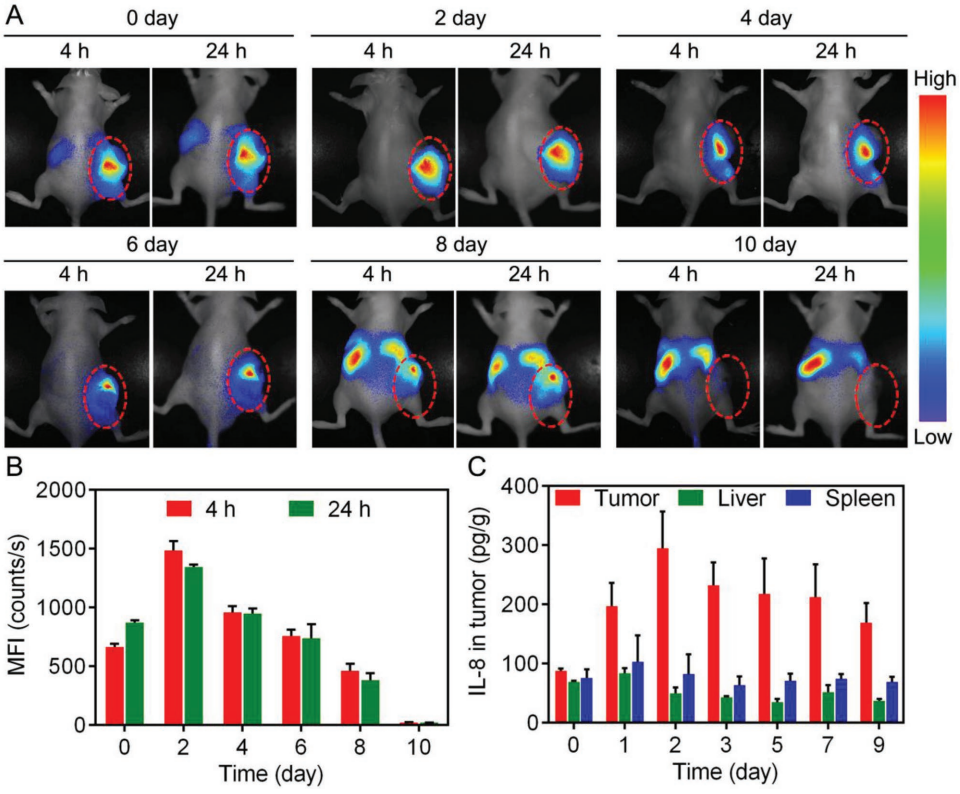

Figure 4. The duration of IMAT for drug-loaded NEs after treatment with one-time PTT. A) In vivo images of DiR-CL/NEs at different time points after one-time PTT. B) The mean fluorescence intensity of tumor site after DiR-CL/NE administration at different time points. C) The duration of IL-8 expression in tumor, liver, and spleen after one-time PTT. The data are shown as the mean ± s.d. ($n = 3$).

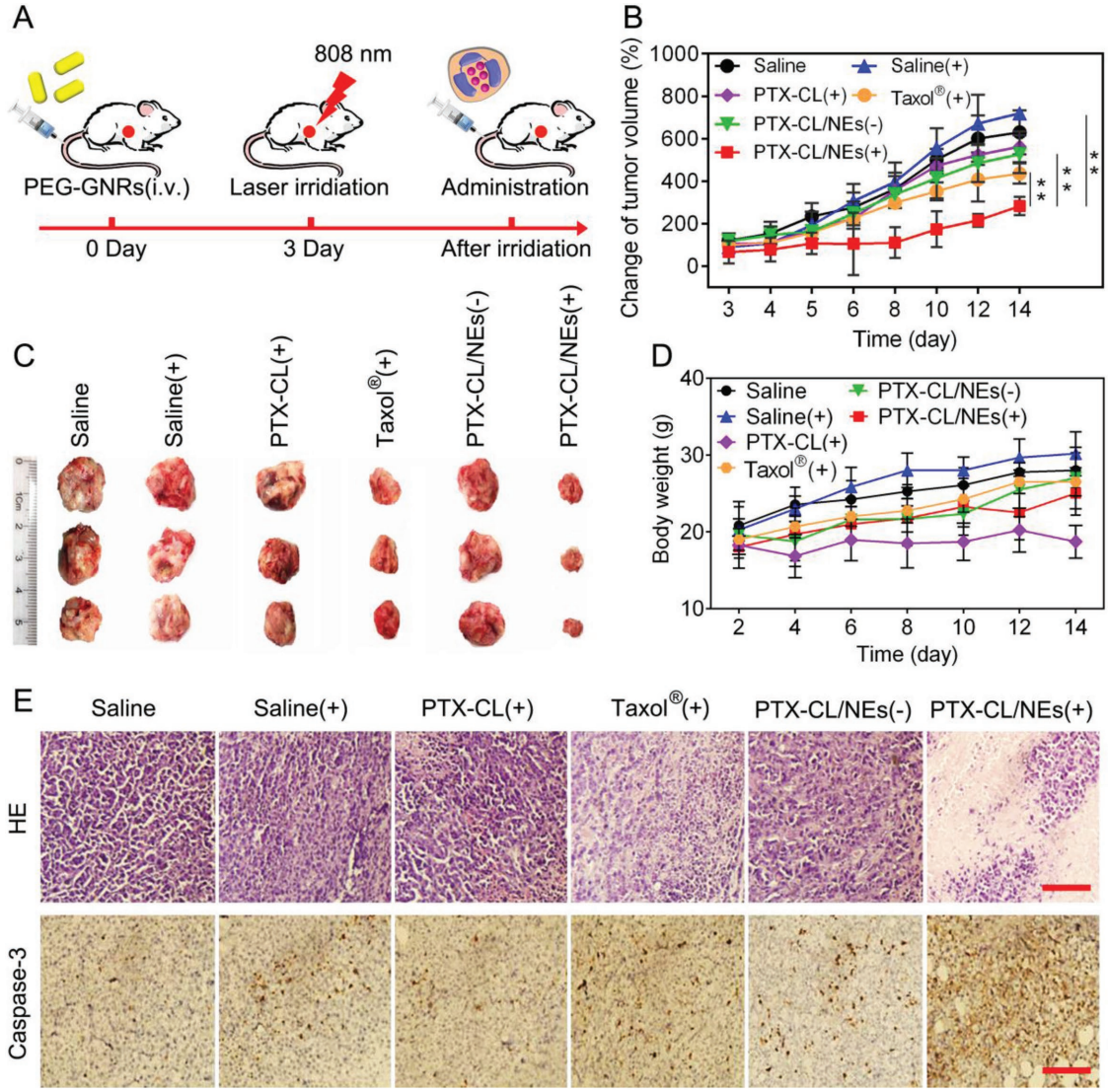

Figure 5. The synergistic therapeutic efficiency of PTT and IMAT chemotherapy. A) Schematic illustration of the procedure of administration in vivo. All mice were administered PEG-GNRs and treated with (+) or without (–) laser irradiation. Mice subsequently received different treatments of saline, PTX-CL, Taxol, or PTX-CL/NEs. B) The growth profiles of HepS tumors in mice that received different treatments. The tumor sizes were monitored by a digital caliper, and the tumor volume was calculated according to the following formula: width^2 × length × 0.5. C) Representative pictures of HepS tumors that received different treatments ($n = 3$). D) Body weight changes in mice that received different treatments. E) The HE staining (top row) and immunohistochemical staining (caspase-3, bottom row) of tumor sections at day 14 after administration of different treatments. Scale bar: 200 µm.

cells were also evaluated. The fluorescence dye of coumarin 6 (C6) was loaded into cationic liposomes (C6-CL) to construct C6-CL/NEs. As shown in Figure S8A (Supporting Information), after being cocultured with the human hepatoma cell line HepG2 for 4 h, the fluorescent dyes of C6 could transfer from C6-CL/NEs to HepG2. A stronger fluorescence signal of C6 in the cytoplasm of HepG2 was detected when treated with phorbol myristate acetate (PMA). The enhanced cargo transfer should be due to the acceleration of C6-CL released from C6-CL/NEs along with the NET formation after PMA stimulation because the DNA content in the supernatant of the release medium significantly increased (Figure S8B,C, Supporting Information).[19] Moreover, the cellular apoptosis study was conducted to evaluate the in vitro synergistic therapy. The results demonstrated that combining PTT with PTX-CL/NEs [PTX-CL/NEs (+)] could induce more tumor cell apoptosis compared to PTT alone [Saline (+)] and chemotherapy alone [PTX-CL/NEs (–)] (Figure S9, Supporting Information). The enhanced cellular inhibition of PTX-CL/NEs (+) would be due to PTT ablation of HepG2 and chemotherapy after PTX transferring into HepG2.

Finally, the in vivo synergistic therapy of PTT with PTX-CL/NEs was also evaluated. PEG-GNRs were first intravenously injected into HepS-tumor-bearing mice, and the tumor was exposed to 2 W cm^{-2} 808 nm laser irradiation for 5 min at 72 h postinjection. After irradiation, saline, PTX-CL, Taxol, or PTX-CL/NEs were intravenously injected, and the tumor volume and body weight of the mice were monitored (**Figure 5**A). As shown in Figure 5B,C, the PTT effect alone

[Saline (+)] suppressed tumor growth only in the first 3 d. Tumor regeneration was observed afterward as the plateau temperature at the tumor sites after one-time PTT was not sufficient for penetration into the deep tumor tissue and only induced part of the tumor to undergo apoptosis and necrosis.[3a,5b] It has been reported that the surviving cancer cells from PTT would further lead to cancer relapse or even accelerate tumor regeneration.[5,9] In contrast, PTT with PTX-CL/NEs [PTX-CL/NEs (+)] displayed a potent tumor inhibition capability compared to PTT alone (Saline (+)) and chemotherapy alone [PTX-CL/NEs (−)], even to PTT with PTX-CL [PTX-CL(+)] or Taxol [Taxol (+)]. The enhanced chemotherapy for PTX-CL/NEs (+) would be the result of the IMAT effect of PTX-CL/NEs, resulting in an increasing recruitment of PTX-CL/NEs into the tumor site. Under the upregulation of inflammatory factors induced by photothermal therapy, PTX-CL/NEs would be intent to break down their nuclear contents and release NETs,[13] which facilitated the release of PTX-CL from NEs for effective chemotherapy. These NETs might undergo degradation by the nuclease, and the dead NEs would likely be eliminated by macrophages in the tumor tissue.[6,20] The HE staining of the tumor section showed serious cell death in the PTX-CL/NEs (+) group. Furthermore, caspase-3 immunohistochemical staining of the tumor section also suggested apparent caspase-3 activation in the PTX-CL/NEs (+) group compared to the other groups, which was commensurate with the observations from HE staining (Figure 5E). These findings indicated a potent tumor inhibition efficacy of our synergistic strategy by combining PEG-GNRs for PTT with PTX-CL/NEs for IMAT chemotherapy. Moreover, the systemic toxicity of this synergistic strategy was evaluated by monitoring the body weight of the mice and a blood biochemical assay after treatment. As shown in Figure 5D, no body weight loss was identified following treatment with PTX-CL/NEs (+); moreover, the liver-enzyme levels of PTX-CL/NEs (+) in the serum were similar to those of saline (Figure S10, Supporting Information), which suggests that PTX-CL/NEs (+) have no serious systematic toxicity.

In summary, we have developed a synergistic anticancer system that combines PTT of PEG-GNRs and the following IMAT chemotherapy of cytopharmaceuticals. Accompanied by hyperthermia to ablate cancer cells, PTT-induced inflammation could facilitate cytopharmaceuticals to migrate toward the tumor area along the chemotactic gradient. This IMAT strategy enhanced the specific accumulation of chemotherapy drugs in the cancer site and broke through the limitation of other active targeting strategies that rely on the recognition between targeting moieties and cell-surface markers. The synergistic anticancer system maximized the anticancer effects by taking advantage of both methods, as well as overcoming the weakness of PTT and chemotherapy. We believe this work further broadens the repertoire of therapy-induced inflammation, which is typically suppressed at clinical treatments. We anticipate the generalization of this method to additional disease treatments in which inflammation is inevitable.

Supporting Information

Supporting Information is available from the Wiley Online Library or from the author.

Acknowledgements

L.Z. and Y.Z. contributed equally to this work. This work was supported by the National Natural Science Foundation of China (81773664, 81473153, and 81503006), the Natural Science Foundation of Jiangsu Province (BK20150698), the National Basic Research Program of China (2015CB755504), the 111 Project from the Ministry of Education of China and the State Administration of Foreign Expert Affairs of China (Grant No. 111-2-07, B17047), the Open Project of State Key Laboratory of Natural Medicines (No. SKLNMZZCX201811), the "Double First-Class" University project (CPU2018GF10), and the Opening Project of Key Laboratory of Drug Targeting and Drug Delivery System, Ministry of Education (Sichuan University). The authors thank the public platform of the State Key Laboratory of Natural Medicines for assistance with HPLC, confocal microscopy, and flow cytometry. The animal protocols used in this study were approved by the Animal Ethics Committee of China Pharmaceutical University.

Conflict of Interest

The authors declare no conflict of interest.

Keywords

combination cancer therapy, cytopharmaceuticals, inflammation, neutrophils, photothermal therapy

Received: September 12, 2018
Revised: November 14, 2018
Published online:

[1] J. Kim, J. Kim, C. Jeong, W. J. Kim, *Adv. Drug Delivery Rev.* **2016**, *98*, 99.

[2] a) Q. Chen, L. Xu, C. Liang, C. Wang, R. Peng, Z. Liu, *Nat. Commun.* **2016**, *7*, 13193; b) W. I. Choi, J. Y. Kim, C. Kang, C. C. Byeon, Y. H. Kim, G. Tae, *ACS Nano* **2011**, *5*, 1995; c) K. F. Chu, D. E. Dupuy, *Nat. Rev. Cancer* **2014**, *14*, 199; d) W. Li, J. Peng, Q. Yang, L. Chen, L. Zhang, X. Chen, Z. Qian, *Biomater. Sci.* **2018**, *6*, 1201.

[3] a) G. von Maltzahn, J. H. Park, A. Agrawal, N. K. Bandaru, S. K. Das, M. J. Sailor, S. N. Bhatia, *Cancer Res.* **2009**, *69*, 3892; b) Y. Hu, C. Chi, S. Wang, L. Wang, P. Liang, F. Liu, W. Shang, W. Wang, F. Zhang, S. Li, H. Shen, X. Yu, H. Liu, J. Tian, *Adv. Mater.* **2017**, *29*, 1700448; c) T. Ma, L. Tan, H. Shao, T. Liu, Y. Xu, Y. Cui, X. Wang, J. Jiang, H. Yu, L. Gao, D. Hong, W. Xu, K. Xu, R. Liu, X. Meng, *J. Biomed. Nanotechnol.* **2017**, *13*, 795; d) W. Song, Y. Li, Y. Wang, D. Wang, D. He, W. Chen, W. Yin, W. Yang, *J. Biomed. Nanotechnol.* **2017**, *13*, 1115; e) T. Wang, Y. Song, W. Zhang, Z. Wu, F. Li, Y. Su, Y. Yang, F. Li, P. Chen, J. Wang, Q. Wu, X. Sun, Y. Lu, D. Ling, *J. Biomed. Nanotechnol.* **2017**, *13*, 1435.

[4] J. Peng, Y. Xiao, W. Li, Q. Yang, L. Tan, Y. Jia, Y. Qu, Z. Qian, *Adv. Sci.* **2018**, *5*, 1700891.

[5] a) C. Wang, L. Xu, C. Liang, J. Xiang, R. Peng, Z. Liu, *Adv. Mater.* **2014**, *26*, 8154; b) Z. Li, H. Huang, S. Tang, Y. Li, X. F. Yu, H. Wang, P. Li, Z. Sun, H. Zhang, C. Liu, P. K. Chu, *Biomaterials* **2016**, *74*, 144.

[6] E. Kolaczkowska, P. Kubes, *Nat. Rev. Immunol.* **2013**, *13*, 159.

[7] a) R. Chen, X. Wang, X. Yao, X. Zheng, J. Wang, X. Jiang, *Biomaterials* **2013**, *34*, 8314; b) J. P. Erinjeri, C. T. Thomas, A. Samoilia, M. Fleisher, M. Gonen, C. T. Sofocleous, R. H. Thornton, R. H. Siegelbaum, A. M. Covey, L. A. Brody, W. Alago Jr., M. Maybody, K. T. Brown, G. I. Getrajdman, S. B. Solomon, *J. Vasc. Interventional Radiol.* **2013**, *24*, 1105; c) F. Ahmad,

G. Gravante, N. Bhardwaj, A. Strickland, R. Basit, K. West, R. Sorge, A. R. Dennison, D. M. Lloyd, *Am. J. Surg.* **2010**, *200*, 500; d) M. Y. Ali, C. F. Grimm, M. Ritter, L. Mohr, H. P. Allgaier, R. Weth, W. O. Bocher, K. Endrulat, H. E. Blum, M. Geissler, *J. Hepatol.* **2005**, *43*, 817; e) A. M. Fietta, M. Morosini, I. Passadore, A. Cascina, P. Draghi, R. Dore, S. Rossi, E. Pozzi, F. Meloni, *Hum. Immunol.* **2009**, *70*, 477.

[8] H. C. Diddens-Tschoeke, G. Huttmann, A. D. Gruber, R. H. Pottier, H. Hanken, *Lasers Surg. Med.* **2015**, *47*, 452.

[9] Q. Dong, X. Wang, X. Hu, L. Xiao, L. Zhang, L. Song, M. Xu, Y. Zou, L. Chen, Z. Chen, W. Tan, *Angew. Chem., Int. Ed.* **2018**, *57*, 177.

[10] J. Xue, Z. Zhao, L. Zhang, L. Xue, S. Shen, Y. Wen, Z. Wei, L. Wang, L. Kong, H. Sun, Q. Ping, R. Mo, C. Zhang, *Nat. Nanotechnol.* **2017**, *12*, 692.

[11] a) D. Chu, J. Gao, Z. Wang, *ACS Nano* **2015**, *9*, 11800; b) D. Chu, X. Dong, X. Shi, C. Zhang, Z. Wang, *Adv. Mater.* **2018**, *30*, 1706245.

[12] a) K. G. Reuter, J. L. Perry, D. Kim, J. C. Luft, R. Liu, J. M. DeSimone, *Nano Lett.* **2015**, *15*, 6371; b) D. R. Elias, A. Poloukhtine, V. Popik, A. Tsourkas, *Nanomed.: Nanotechnol., Biol. Med.* **2013**, *9*, 194.

[13] B. Geering, H. U. Simon, *Cell Cycle* **2011**, *10*, 2821.

[14] E. C. Dreaden, M. A. Mackey, X. Huang, B. Kang, M. A. El-Sayed, *Chem. Soc. Rev.* **2011**, *40*, 3391.

[15] a) G. von Maltzahn, J. H. Park, K. Y. Lin, N. Singh, C. Schwoppe, R. Mesters, W. E. Berdel, E. Ruoslahti, M. J. Sailor, S. N. Bhatia, *Nat. Mater.* **2011**, *10*, 545; b) L. Vigderman, B. P. Khanal, E. R. Zubarev, *Adv. Mater.* **2012**, *24*, 4811; c) J. H. Park, G. von Maltzahn, L. L. Ong, A. Centrone, T. A. Hatton, E. Ruoslahti, S. N. Bhatia, M. J. Sailor, *Adv. Mater.* **2010**, *22*, 880.

[16] a) J. A. Barreto, W. O'Malley, M. Kubeil, B. Graham, H. Stephan, L. Spiccia, *Adv. Mater.* **2011**, *23*, H18; b) G. Song, L. Cheng, Y. Chao, K. Yang, Z. Liu, *Adv. Mater.* **2017**, *29*, 1700996.

[17] M. F. Meza, M. A. Kates, R. W. Barbee, S. Revall, B. Perry, J. P. Murgo, J. Cheirif, *J. Am. Coll. Cardiol.* **1997**, *29*, 974.

[18] S. J. Galli, N. Borregaard, T. A. Wynn, *Nat. Immunol.* **2011**, *12*, 1035.

[19] a) V. Papayannopoulos, *Nat. Rev. Immunol.* **2017**, *18*, 134; b) G. D. Katkar, M. S. Sundaram, S. K. NaveenKumar, B. Swethakumar, R. D. Sharma, M. Paul, G. J. Vishalakshi, S. Devaraja, K. S. Girish, K. Kemparaju, *Nat. Commun.* **2016**, *7*, 11361.

[20] V. Papayannopoulos, *Nat. Rev. Immunol.* **2018**, *18*, 134.